Multi-Objective Optimization of EE-core Transformers using Geometric Programming

Tim Mcrae, Andrija Stupar, Thierry Meynard

Multi-Objective Optimization of EE-core Transformers using Geometric Programming

Tim McRae
Centre for Industrial Electronics
University of Southern Denmark
Sønderborg, Denmark
mcrae@sdu.dk

Andrija Stupar
Eneropta Corp.
Toronto, Canada
andrija@stupar.com

Thierry Meynard
Laboratoire LAPLACE, ENSEEIHT
INPT, University of Toulouse
Toulouse, France
meynard@laplace.univ-tlse.fr

Abstract—This paper introduces a generalized optimization algorithm for the design of EE-core based transformers using geometric programming. The objective functions, loss and volume, and the constraints must be either posynomials (positive polynomials) or monomials (products of variables with exponents) to conform to the requirements of geometric programs. We can optimize transformers and generate a set of optimal solutions to construct a Pareto front based on inputs from a user. The algorithm, modelling and constraints are described. The output of the optimization has been compared to an experimental prototype to characterize the validity of the models.

Index Terms—Transformers, Convex Optimization, Modelling, Magnetics

I. Introduction

Magnetics are an integral component of power electronics but they are challenging to design in general as they are highly dependent on material parameters, geometry, and cost [1]. Some aspects, including proximity effects, effective air gap length, and fringing fields, have no closed form equations. As a result losses are difficult to predict without the use of numerical analysis and computational methods [2], [3]. Convex optimization techniques (geometric programming (GP) [4]) have been used in [5] and [6] to design inductors, but have not yet been applied to transformers. The results for inductor design indicate we can improve the transformer design process. GPs guarantee a globally optimum solution in a convex design space and significantly reduces solution times compared to other optimization techniques [5] but require objectives and constraints to be either posynomial or monomial functions. A multi-objective optimization can be achieved by varying the relative importance of losses and volume over several optimization cycles, generating a family of Pareto optimal solutions. This gives a geometric program of the form

$$\begin{aligned} &\text{minimize} && \gamma\frac{P_{total}}{P_{max}} + (1-\gamma)\frac{Vol_{total}}{Vol_{max}}, \\ &\text{subject to} && f_i \le a_i, \text{ for i from 1 to n} \end{aligned} \tag{1}$$

where P_{total} is the total loss of the magnetic device, P_{max} is the maximum loss solution given the design constraints, Vol_{total} the total volume of the magnetic device, Vol_{max} is the maximum volume solution given the design constraints, γ the relative weighting factor of these two optimization goals, and the f_is are the constraint functions of the design problem.

The method of [5] has been modified and extended to create a convex GP model of EE-core transformers. The optimization algorithm is designed to account for different winding arrangements through an iterative process. This algorithm improves upon [5] by using the iterated optimizations to generate constraints using non-posynomial functions. CVX, a convex optimization tool, is used to solve these problems [7], [8].

II. Principle of Operation

The optimization algorithm developed here focuses on EE-core transformers. Several equations in transformer design are already in monomial or posynomial form. The correction factors F_r and G_r for conduction and proximity loss respectively derived in [9] are not posynomial and must be approximated using fits. A max-monomial fit algorithm described in [5] was used. An arctangent model was used to account for core saturation [10]. Reluctance, magnetic permeability, and core loss are generated through curve fitting from data sets created from simulation in the SIMPLIS Magnetic Design Module (MDM) [11] for ferrite core materials 3C81 and N87. Constraints are developed based on core geometry, temperature, magnetic field and magnetic flux density, and current density requirements. The required inputs are shown in Table I and the variables of optimization are given in Table II. The number of turns per winding is optimized as a continuous variable

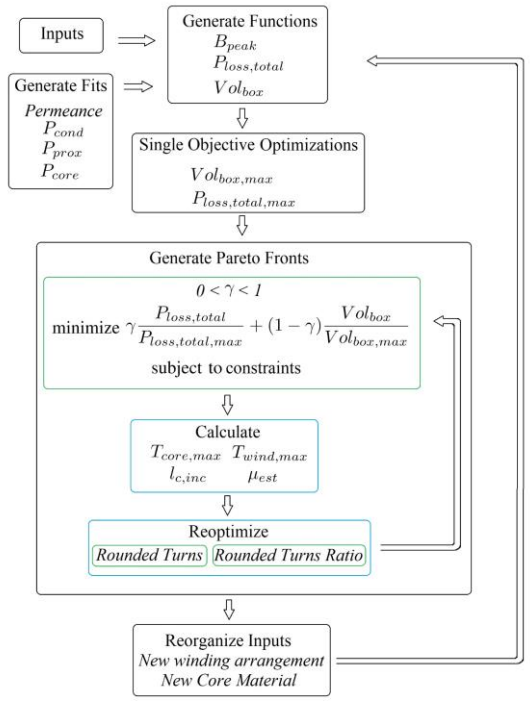

(a)

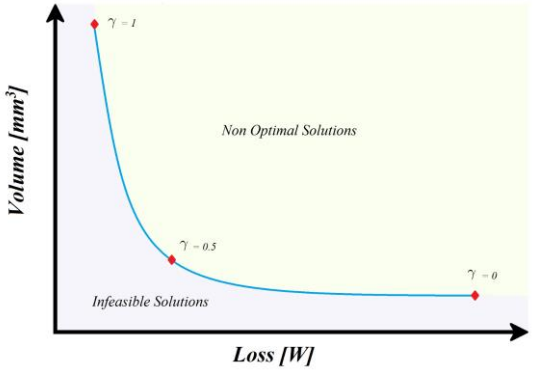

(b)

Fig. 1: a) Overall structure of the optimization algorithm and b) an example output of a single pass of the algorithm.

then rounded. To create a Pareto front we use a factor γ to vary the relative weight between loss and volume. At each value of γ the optimization is run and the solutions are connected. A diagram of this process and the expected output for a single choice of core material and winding arrangement can be seen in Fig. 1.

The value γ should only be considered an internal variable used to construct the Pareto front. The fact that this is a multi-objective problem implies that there is a trade-off between these two objectives. Allowing more loss in the final design may allow a smaller implementation and vice versa. However, when constructing a transformer, the design may have a maximum allowable volume/footprint or loss. This places a limit on the set of designs and may result in a single reasonable optimal solution. We can imagine these additional constraints as a vertical or horizontal lines in the solution space seen in Fig. 1b and the optimal solutions are intersections of these lines with the Pareto front.

To overcome the limitation of non-convexity of magnetic permeability and core temperature, these variables are calculated directly between optimization steps in the calculation of the Pareto front.

Table I: Inputs

Variable	Value [unit]
L_{mag}	Magnetizing Inductance $[H]$
Turns Ratio	Relative turns of each winding [vector]
I_{ripple}	Amplitude of AC component $[A$, vector$]$
I_{DC}	Amplitude of DC component $[A$, vector$]$
waveforms	Waveshape of current [#, vector]
V_{in}	Input Voltage $[V]$
vwave	Applied voltage waveform [#]
Duty Ratio	Duty of each winding [#, vector]
f_{sw}	Switching Frequency $[Hz]$
σ	Conductivity $[siemens/mm$, vector$]$
Magnetic Material	Material Choice $[String$, vector$]$
Saturation Percent	Maximum allowable saturation [#]
$Core_{asp}$	Core aspect ratio [#]
$Wind_{asp}$	Window aspect ratio [#]
T_{amb}	Ambient Temperature $[°C]$
Gapped	Is the core gapped $[binary]$
Flyback	Is this a flyback transformer $[binary]$

Table II: Optimization Variables

Variable	Value [unit]
A_c	Effective Core Area $[mm^2]$
W_a	Effective Window Area $[mm^2]$
l_eff	Effective Core Path Length $[mm]$
l_c	Effective Core Cross Sectional Length $[mm]$
w_c	Effective Core Cross Sectional Width $[mm]$
l_w	Effective Window Length $[mm]$
w_w	Effective Window Width $[mm]$
d	Wire Diameter/winding (vector) $[mm]$
s	Wire Insulation Thickness/winding (vector) $[mm]$
t	Tape Insulation Thickness/winding (vector) $[mm]$
wa	Wire area/winding (vector) $[mm^2]$
ia	Insulation area/winding (vector) $[mm^2]$
nl	Number of layers * wire diameter/winding (vector) $[mm]$
$Core_{circ}$	core circumference $[mm]$
$Wind_{circ}$	Window circumference $[mm]$
MLT	Mean Turn Length $[mm]$
N	Turns Ratio Scaling Factor [#]
gap	Gap Length $[mm]$
μ_r	Relative Permeability [#]
T_c	Core Temperature $[°C]$
T_w	Winding Temperature $[°C]$
H_{DC}	DC Bias Field $[A/m]$

The full GP Is

$$\text{minimize } \gamma \frac{P_{loss,total}}{P_{loss,total,max}} + (1-\gamma)\frac{Vol_{box}}{Vol_{box,max}} \quad (2)$$

subject to $T_{amb} + (P_{cond} + P_{prox})R_{th,wind} \leq T_{wind}$,

$$\begin{aligned}
&T'_{wind} \leq 1.1T_{wind,est}, T_{wind} \leq T_{wind,max}\\
&0.99T'_{wind} \leq T_{wind} \leq 1.1T'_{wind},\\
&T_{amb} + P_{core}R_{th,core} \leq T'_{core},\\
&T'_{core} \leq 1.1T_{core,est}, T_{core} \leq T_{core,max},\\
&0.99T'_{core} \leq T_{core} \leq 1.1T'_{core},\\
&L_{mag,des} = N^2\frac{e^{\alpha_1}A_c^{\alpha_2}W_a^{\alpha_3}\mu_r^{\alpha_4}}{gap^{\alpha_5}l_e^{\alpha_6}},\\
&B_{peak} + \mu H_{DC} \leq min(B_{sat}, B_{max}),\\
&H_{DC} = \frac{N_{prim}I_{mag,dc}}{l_{eff}}, \mu = \mu_{est},\\
&A_e = l_c w_c, W_a = l_w w_w,\\
&core_{circ} = 2(1 + core_{asp})w_c,\\
&l_c = core_{asp}w_c, l_w = window_{asp}w_w,\\
&window_{circ} = 2(1 + window_{asp})w_w,\\
&l_{eff} = 2(1 + window_{asp})w_w l_{core,inc},\\
&A_{w,i} \geq N_{turns,i}\frac{\pi d_i^2}{4},\\
&A_{ins,i} \geq N_{turns,i}\pi d_i s_i,\\
&n_{l,i} \geq N_{turns,i}\frac{d_i^2}{l_w} + d_i,\\
&1.1\sum n_{l,i} \leq w_w, 1.1d \leq l_w\mathbf{1},\\
&\sum A_w + \sum A_{ins} \leq 0.9 l_w w_w,\\
&MLT_1 \geq core_{circ} + \pi(\frac{d_1}{2} + s_1 + t_1),\\
&MLT_i \geq MLT_{i-1} + \pi(\frac{d_i}{2} + s_i + t_i),\\
&d_i \geq 2\sqrt{\frac{I_i + I_{DC,i} + I_{refl,i}}{\pi J_{max}}}
\end{aligned}$$

This single transformer optimization is the kernel of a larger optimization which considers two additional factors: winding arrangements and core material. The algorithm generates Pareto fronts for several winding arrangements by dividing windings into layers and permuting the ordering of the layers. The winding with the highest current-turns is placed closest to the core first. The next optimization splits windings in two and reorders the windings based on largest current by number of windings. Pareto fronts for each desired core material are also constructed. The total optimization can be seen in Fig. 1a.

Currently there are two configurations. The first orders the windings (3) based on the highest current so that the highest current turns are nearest to the core in an effort to reduce conduction loss.

$$N_{turns,1}I_1 > N_{turns,2}I_2 > \ldots > N_{turns,i}I_i \quad (3)$$

The next optimization assumes some maximum threshold for the maximum turns ratio (not actual turns because N is determined after optimization). If the value in the turns ratio vector is greater than 5, that winding is split into two windings. If the division results in a fraction, the winding nearer to the core is rounded up and the other rounded down. These windings are connected in series. The optimizer can interleave primary and secondary windings by specifying the order in the turns ratio vector. In other words, different winding structures can be compared, but the optimizer does not decide what the optimal winding arrangement should be. The distribution of the turns of each winding around the core is not specified as the optimizer considers and average of each winding. Paralleling secondary side windings is possible by simply adding new windings to the turns ratio vector. The designer can then connect these windings in parallel when building the transformer. Paralleling of the primary windings is not implemented because the optimizer assumes all primary windings are connected in series.

A. Extension to Other Core Geometries

This method can be extended to different core geometries by adjusting the geometric and reluctance constraints. The underlying geometric model (seen in Fig. 2) shows how the constraints were constructed for the EE core. Core dimensions for a different core geometry can be used to define core and gap reluctance, core area, window area. Equations for different wire geometries could also be included but new fits for AC conduction loss and proximity loss would be needed.

III. Models and Constraints

A. Volume

There are two volumes of interest for transformers: the volume of the core material, which is used to calculate core losses, and the boxed volume, used to calculate how much volume the transformer occupies. The model of an E-core transformer used for optimization can be seen in Fig. 2. While general E-cores can have several dimensions, the core of interest is simplified so that it can be described by four variables, l_c, w_c, l_w, and w_w. The side legs and top/bottom bars of the transformer are assumed to have half the cross-sectional area of the centre leg so that flux divides evenly and so that all parts of the core reach a similar maximum flux density for a given set of operating conditions. The boxed volume of the core is simply the multiplication of length,

width and depth and is shown in Eq. 4. The core volume is the boxed volume less the volume of the winding window. It is given in Eq. 5.

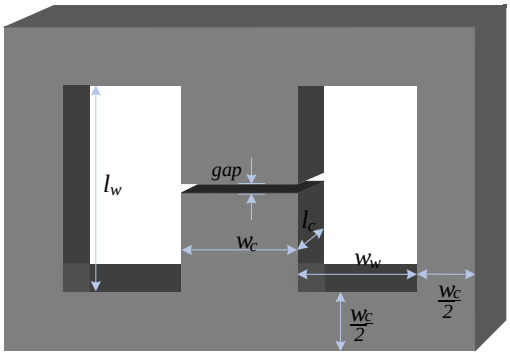

Fig. 2: Transformer EE-core geometry.

$$Vol_{core,box} = l_c(w_c + l_w)(2w_c + 2w_w) \quad (4)$$

$$Vol_{core} = 2l_c w_c(l_w + w_c + w_w) \quad (5)$$

where the variables are described in Table II.

The total boxed volume (6) is calculated using this and the geometry of the transformer windings. The surface area of the front face of the transformer is multiplied by the total length the windings extended from the core and multiplied by 2 to account for the front and the back.

$$Vol_{box} = Vol_{core,box} + 2(\sum_i (d_i + 2s_i)\frac{n_{l,i}}{d_i} + t_i)(2w_w + 2w_c)(l_w + w_c) \quad (6)$$

B. Loss

Total loss (7) is divided into three components: conduction loss (8), proximity loss (9), and core loss (10). There were no partitions for the skin and proximity loss coefficient F_r and G_r fits.

$$P_{loss,total} = P_{conduction} + P_{proximity} + P_{core} \quad (7)$$

The conduction loss for a single winding takes the form:

$$P_{conduction} = I_{ripple}^2 \frac{4MLTN_{Turns}}{\pi d^2} \cdot (1 + k_{th,copper}(T_w - T_a))\sqrt{\frac{\mu_0}{\sigma\pi^\alpha}} C_{harmonics} \cdot \sum_{i=1}^{4} e^{k_{Fr,4i-3}} f_{sw}^{k_{Fr,4i-2}+0.5} d^{k_{Fr,4i-1}-1} \sigma^{k_{Fr,4i}} \quad (8)$$

where the first term represents the square of the current times the DC resistance of the winding. N_{turns} is the number of turns of that winding. The next term accounts for variation of resistance with temperature. The radical accounts for skin effect, with the frequency term being placed into the posynomial fit. $C_{harmonics}$ is a coefficient derived from summing harmonics for different waveforms, and $k_{Fr,j}$ are the posynomial fit coefficients for skin effect factor F_r found in [9].

Proximity loss for a single winding takes the form:

$$P_{proximity} = I_{ripple}^2 \frac{4MLTN_{Turns}}{\pi d^2} \cdot (1 + k_{th,copper}(T_w - T_a))((N_{Turns})^3 \cdot (n_l)^3/d^3/l_w^2/3)\sqrt{\frac{\mu_0}{\sigma\pi^\alpha}} C_{harmonics} \cdot \sum_{i=1}^{6} e^{k_{Gr,4i-3}} f_{sw}^{k_{Gr,4i-2}} d^{k_{Gr,4i-1}} \sigma^{k_{Gr,4i}} \quad (9)$$

where the first term is the square of the current times the DC resistance of the winding. The next term accounts for changes in resistance due to temperature.

N_{Turns} is the number of turns and n_l is the number of layers multiplied by the wire diameter. These terms arise from factoring and relaxing the equation from [9] to make it convex. The radical accounts for skin effect and $C_{harmonics}$ is a coefficient derived from summing harmonics for different waveforms. $k_{Gr,j}$ are the posynomial fit coefficients for the factor G_r found in [9].

For the core loss (10), harmonics are also summed for each waveform.

$$P_{core} = Vol_{core} C_{harmonics} \cdot 8 \text{X} e^{k_{core,5i-4}} \Delta B^{k_{core,5i-3}} f_{sw}^{k_{core,5i-2}} H_{DC}^{k_{core,5i-1}} T_{core}^{k_{core,5i}} i=1 \quad (10)$$

where $k_{core,j}$ are the posynomial fit coefficients. Currently there are only coefficients for $3C81$ and $N87$ and they are fit with 6 terms.

As the intention is that the total loss equation can account for any number of windings, a new loss function is automatically generated before the first optimization takes place.

C. Inductance and Field Constraints

The core permeance was used to calculate final magnetizing inductance in place of reluctance. Permeance was modelled by summing each straight core section as described in [9].

$$L_{mag,des} = N_{turns,prim}^2 \frac{e^{\alpha_1} A_c^{\alpha_2} W_a^{\alpha_3} \mu_r^{\alpha_4}}{gap^{\alpha_5} l_e^{\alpha_6}} \quad (11)$$

where α_j are the monomial fit coefficients. The user can select between a gapped and non-gapped core, which changes the permeance model. We can see here directly that a monomial fit has an asymptote at zero gap

length for a gapped core. For this reason, minimum gap length requires a minimum greater than 2 μm.

An arctangent model is used to describe the B-H curve [10]. The coefficients for this model are derived from collected simulation data.

$$B = \frac{\mu_0 \mu_a}{k_{mag}} arctan(k_{mag} H) \tag{12}$$

where μ_a is the amplitude permeability and k_{mag} is a coefficient to fit the arctangent model to the desired magnetic material. This model does not describe hysteresis and is instead used to account for core saturation. At the beginning of the algorithm, a B_{peak} function is generated based on integrating the applied voltage waveform. Two constraints are placed here, one for an explicit maximum flux density selected by the designer or by a saturation percentage.

$$B_{peak} + \mu H_{DC} < min(B_{max}, B_{sat}) \tag{13}$$

H_{DC} determines the DC operating point on the B-H curve, which determines what maximum AC flux density is possible before reaching the predetermined saturation limit, as well the relative permeability.

$$H_{DC} = \frac{N_{turns,prim} I_{mag,dc}}{l_{eff}} \tag{14}$$

The equation for relative permeability is the derivative of the arctangent model of the B-H curve, seen in (15). Unfortunately, this equation is neither convex nor concave and cannot be used as a lower bound in the constraints. The relative permeability is instead estimated from previous optimizations outside of the geometric programming framework. Here we use the iterative nature of the Pareto front to overcome the convexity requirements of GPs.

$$\mu_{est} = \frac{\mu_0 \mu_a}{1 + (k_{mag} H_{DC})^2} \tag{15}$$

D. Geometric Constraints

The constraints here (16)-(23) are primarily maximums and minimums on core area, window area, wire thickness, tape thickness and insulation thickness. The other geometric constraint here is the relation of core area and window area. The core length and width and window length and width independently were defined independently.

$$A_e = l_c w_c, \tag{16}$$

$$core_{circ} = 2(1 + core_{asp}) w_c, \tag{17}$$

$$l_c = core_{asp} w_c, \tag{18}$$

$$W_a = l_w w_w, \tag{19}$$

$$window_{circ} = 2(1 + window_{asp}) w_w, \tag{20}$$

$$l_w = window_{asp} w_w, \tag{21}$$

$$l_{eff} = 2(1 + window_{asp}) w_w l_{c,inc} \tag{22}$$

The $core_{circ}$ and $window_{circ}$ variables were defined to enable calculation of effective path length and MLT.

$$l_{core,inc} = 1 + \frac{2.5 w_c}{2(1 + window_{asp}) w_w} \tag{23}$$

where $l_{core,inc}$ is the increase to the effective path length of the core. The factor of 2.5 comes from the assumed geometry of E cores, and the division by w_{window} is done to cancel out with the multiplication by w_{window} in the l_{eff} equation. This was done to ensure the equality constraint remains a monomial.

E. Winding and Window Constraints

To accommodate for the variable number of windings and layers within windings, internal optimization variables describing the wire area, the insulation area and the number of layers were introduced (24)-(26). These are needed to ensure the window area is not overfilled, and that the windings fit the width of the window (27)-(29). This optimization is effectively restricted to considering shells of windings.

$$A_{w,i} \geq N_{turns,i} \frac{\pi d_i^2}{4}, \tag{24}$$

$$A_{ins,i} \geq N_{turns,i} \pi d_i s_i, \tag{25}$$

$$n_{l,i} \geq N_{turns,i} \frac{d_i^2}{l_w} + d_i \tag{26}$$

These variables enable other constraints to be simply affine or linear constraints. The number of layers is multiplied by the wire diameter for convenience.

$$1.1 \sum n_{l,i} \leq w_{window}, \tag{27}$$

$$1.1 d \leq l_w \mathbf{1}, \tag{28}$$

$$\sum A_w + \sum A_{ins} \leq 0.9 l_w w_w \tag{29}$$

These constraints (27)-(29) guarantee that the windings fit into the window in terms of length, width and overall area.

$$MLT_1 \geq core_{circ} + \pi(\frac{d_1}{2} + s_1 + t_1) \tag{30}$$

$$MLT_i \geq MLT_{i-1} + \pi(\frac{d_i}{2} + s_i + t_i) \tag{31}$$

The MLT constraints (30)-(31) must be dynamically generated to account for the variable number of windings.

Finally, (32) is related to the current density. We wish to ensure that no winding experiences a current density above some J_{max}. As the number of windings is variable, the number of constraints is dynamically allocated.

$$d_i \geq 2\sqrt{\frac{I_i + I_{DC,i} + I_{refl,i}}{\pi J_{max}}} \tag{32}$$

In (32), I_i is the AC component of the winding current, $I_{DC,i}$ is the DC component of the winding current, and $I_{refl,i}$ is the current reflected to that winding (if there is any). This $I_{refl,i}$ is calculated before the optimization takes place. This constraint determines the smallest allowable wire diameter.

IV. Flyback Transformer Optimization Example

An example transformer design for flyback operating in discontinuous conduction mode (DCM) is provided here to demonstrate the design process. A summary of the relevant design parameters is given in Table III. The final Pareto fronts can be seen in Fig. 3. Two separate optimization passes took place, one for the primary winding closest to the core (non-interleaved) and the other where the primary winding is split into two interleaved layers. The most notable thing about these Pareto fronts are the cusps. When the scaling factor or number of turns is rounded, subsets of the solutions are grouped by integer turns and the remaining variables are re-optimized. As the turns shift from one integer to another, the solutions on either side of the boundary may have significantly different constraints to meet, notably inductance and core saturation. This results in jumps in the Pareto front as the solution space changes from one subset to the next. Visualizations of three of the designs, created in SIMPLIS MDM, can be seen in Fig. 4. The details for these three designs are given in Table IV.

V. Experimental Results

Three transformers were designed to test the optimization algorithm. All these transformers are ungapped. To ensure a realizable solution was generated, an optimization was performed and a solution with a core size close to a readily available core size was selected. Then the core size was fixed and the system was reoptimized. This was done for several operating conditions, which can be seen in Table V. The core for each operating condition was chosen to be the same,

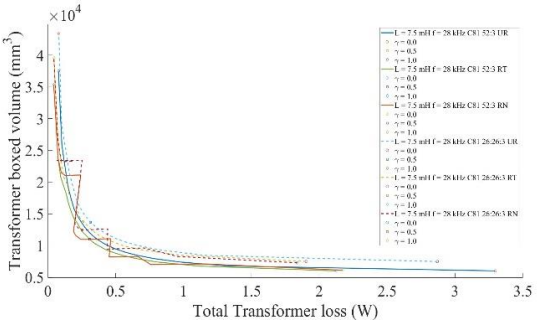

Fig. 3: Pareto front outputs of the DCM Flyback Transformer. UR - Unrounded, RT - Rounded Turns, RN - Rounded N. The first set of numbers is the turns ratio. The two passes that were done were for a 52:3 transformer (the first three Pareto fronts) and a 26:26:3 transformer, where the primary is split into two interleaved layers.

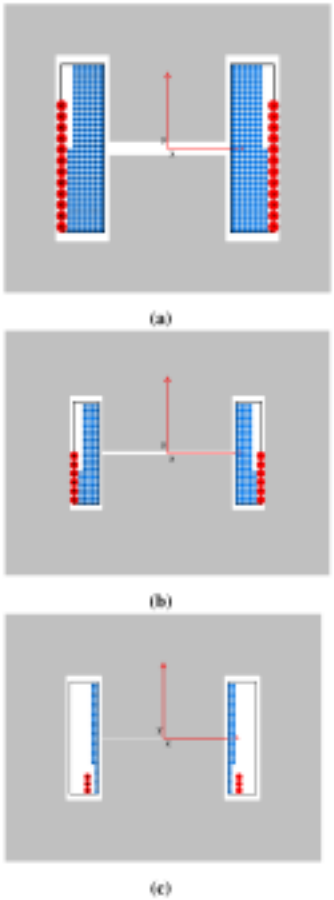

Fig. 4: DCM Flyback transformer designs resulting from the optimization featuring a non-interleaved primary and a turns ratio of 52:3: a) γ = 0.05 (optimized for volume) b) γ = 0.5 (half-way compromise between volume and losses) c) γ = 0.99 (optimized for losses). For dimensions see Table IV.

Table III:
DCM Flyback System Parameters

f_{sw}	$28kHz$
V_{in}	$310V$
L_{mag}	$7.5mH$
D	$[0.25,\ 0.7]$
Turns Ratio	$[-52,\ 3]$
I_{out}	$2A$
T_{amb}	$25°C$
Conductor	copper
Core Material	3C81
Saturation Percent	0.7
Core Aspect Ratio	1
Window Aspect Ratio	3.5

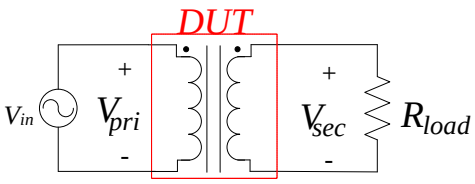

Fig. 5: Circuit diagram of the experimental test setup.

normalizing the core volume across the experiment. The optimizer produced a Pareto set of optimal results for each of the three input conditions. These Pareto fronts are plotted in Fig. 7.

One solution from each set was selected for construction and experimental measurement, and each was approximated by a prototype using available sizes of wire. The dimensions of the prototypes as built for each operating condition are given in Table V. To evaluate these designs, the prototype parameters were used to calculate the losses at each operating condition using the GP model. The three prototype transformers were also modeled in SIMPLIS MDM and simulated at their respective operating conditions. Finally, losses in each of the prototype transformers were measured using a Yokogawa power analyzer with the circuit set up as in Fig. 5. The comparison of the optimizer's GP model loss calculation, the MDM simulation, and the experimental measurement is shown in Table V with a more detailed breakdown given in Fig. 6.

There is a large deviation between the optimizer's loss calculation and the experimental results - 38.7%, 67%, and 38.7% for the three operating conditions, respectively. However, SIMPLIS MDM simulations match the experimental results very well, with errors of 13.6%, 13.4%, and 12.6%. We use MDM to determine sources of error in the optimizer's GP model.

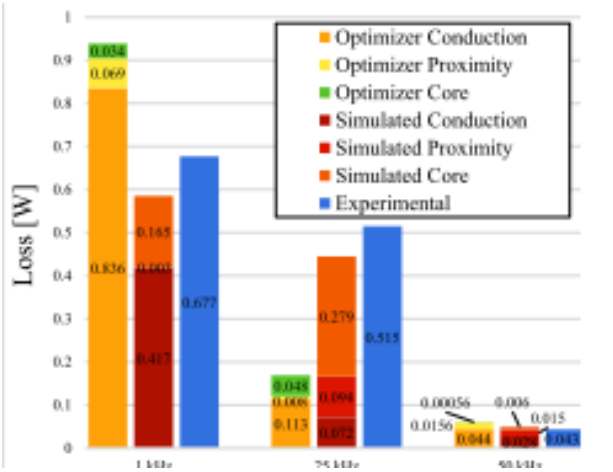

Fig. 6: The detailed loss breakdown and comparison of the calculated, simulated, and measured losses for the three experimental prototypes described in Table V.

As seen in Fig. 6, conduction loss is overestimated in all three cases and core loss is underestimated. The error in conduction loss is most likely caused by the posynomial approximation of the skin effect factor F_r. Similarly there is an error in proximity loss as the proximity loss factor G_r has the most relaxed model due to it being highly non-convex. Several differences between the physical implementation and the optimizer model also exist. For this particular core, the core dimensions deviate from the assumed core dimensions as the side legs are smaller than half the core width. This results in a variation in core volume and boxed volume along with a difference in expected magnetizing inductance. Exact locations of each turn within the winding window are beyond the scope of the optimizer but have an impact on final loss. Conduction and proximity losses are calculated on a winding level, not per turn, which further introduces inaccuracy.

For a more comprehensive comparison, the Pareto sets resulting for each operating condition were simulated in MDM, and are compared to the optimizer results in Fig. 7. The simulated Pareto fronts are shifted compared to the optimization results. However the general shape of the simulated transformers is similar to the GP-calculated Pareto fronts for each of the operating conditions. Although there is an error in the absolute numbers, the similarity in shape demonstrates that a relationship between design variables and the optimizer goal has been identified. Therefore the relative positions of the generated optimal designs on the Pareto front are correct, but real-world measured losses and volumes will be shifted compared to those predicted by the optimizer.

Table IV:
DCM Flyback Transformer Optimization Results

[mm]	h	w	ww	wc	lc	gap	hw	$Turns$	d	P_{loss}[W]	$Volume[mm^3]$
$\gamma = 0.05$	11.4	25.49	16.77	8.717	8.717	1.02	7.05	208:12	[0.3635, 0.802]	0.886	6 054
$\gamma = 0.5$	11.55	30.82	18.49	12.33	12.33	0.293	5.39	104:6	[0.3635, 0.802]	0.315	9 884
$\gamma = 0.99$	17.58	45.0	27.56	17.44	17.44	0.089	8.86	52:3	[0.492,0.953]	0.0465	30 224

Table V:
Experimental Setup and Results

Scope Power Analyzer R_{load}		Teledyne Lecroy HDO4024-MS Yokogawa WT3000 1Ω, 5Ω	
fsw	$1kHz$	$25kHz$	$50kHz$
Turns Ratio	[-22:11]	[-16:2]	[-48:10]
L_{mag}	$7.5mH$	$7.5mH$	$50mH$
$L_{mag,MDM}$	$12.116mH$	$6.409mH$	$57.678mH$
V_{in}	$10V$	$48V$	$24V$
I_{out}	$5A$	$6A$	$1A$
$Core$	E55/28/25	E55/28/25	E55/28/25
Wire Diameters	1 mm, 1.2 mm	1 mm, 1.4 mm	0.5 mm, 0.85 mm
Opt Loss Total	0.939 W	0.17 W	0.06034 W
MDM Loss Total	0.585 W	0.446 W	0.049 W
Exp Loss	0.677 W	0.515 W	0.0435 W

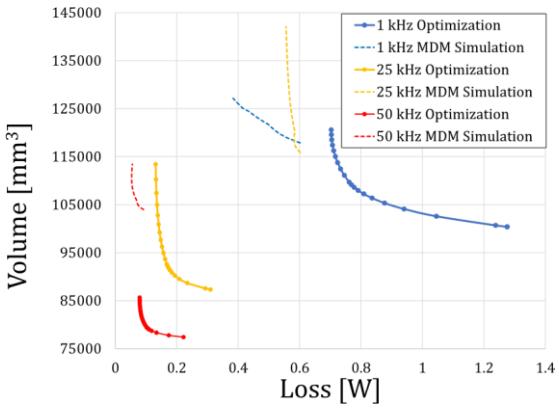

Fig. 7: Comparison between the output from the optimizer and MDM simulation for the 1 kHz, 25 kHz, and 50 kHz designs.

VI. Conclusion

This paper has developed a multi-objective convex optimization problem using geometric programming to aid in the design of EE-core transformers. Models for volume, loss, magnetic fields and geometric constraints have been developed to enable solutions to general transformer design problems. The benefit of the overall optimization framework is that it can be continually improved as the posynomial models of the transformer are improved. A novel method of including non-posynomial functions into the GP optimization framework has been implemented using the iterative nature of Pareto front generation. Since many non-convex models of transformer losses were approximated by posynomial functions, there are significant differences between the losses predicted by the optimizer and experimentally measured losses. While further work needs to be done to refine the posynomial models for skin and proximity effect, a combination of experimental measurements and simulations in SIMPLIS MDM confirms that the optimizer can be used as a tool which points the designer to the proper part of the design space in accordance with the optimization goal, therefore likely reducing the time needed to arrive at a truly optimal design.

References

[1] E. I. Amoiralis, M. A. Tsili, P. S. Georgilakis, A. G. Kladas, and A. T. Souflaris, "A Parallel Mixed Integer Programming-Finite Element Method Technique for Global Design Optimization of Power Transformers," *IEEE Transactions on Magnetics*, vol. 44, no. 6, pp. 1022–1025, 2008.

[2] K. Dawood, G. Komurgoz, and F. Isik, "Modeling of Distribution Transformer for Analysis of Core Losses of Different Core Materials Using FEM," in *2019 8th International Conference on Modeling Simulation and Applied Optimization (ICMSAO)*, 2019, pp. 1–5.

[3] Z. Song, K. Gong, S. Mou, Y. Zhu, B. Xiang, and C. Zhou, "The simulation of stray losses in a power transformer based on FEM," in *2011 International Conference on Electrical and Control Engineering*, 2011, pp. 4199–4201.

[4] S. Boyd, S.-J. Kim, L. Vandenberghe, and A. Hassibi, "A tutorial on geometric programming," *Optim Eng*, vol. 8, pp. 67–127, April 2007.

[5] A. Stupar, D. Flumian, B. Gouedard,´ and T. Meynard, "Generation and Derivation of Practical Optimization-Oriented Models of Inductors," in *COMPEL 2019*, 06 2019, pp. 1–8.

[6] A. Furlan, A. Morentin, G. Fontes, G. Delamare, M. Heldwein, and T. Meynard, "Homothetic Method to Compute Winding Losses in the Design of Power Inductors," 12 2019, pp. 1–6.

[7] M. Grant and S. Boyd, "CVX: Matlab Software for Disciplined Convex Programming, version 2.1," http://cvxr.com/cvx, Mar. 2014.

[8] ——, "Graph implementations for nonsmooth convex programs," in *Recent Advances in Learning and Control*, ser. Lecture Notes in Control and Information Sciences, V. Blondel, S. Boyd, and H. Kimura, Eds. Springer-Verlag Limited, 2008, pp. 95–110, http://stanford.edu/¨boyd/graph dcp.html.

[9] J. V. Muhlethaler, "Modeling and multi-objective optimization of¨ inductive power components," Zurich, 2012.¨

[10] R. Szewczyk, "Technical B-H saturation magnetization curve models for SPICE, FEM and MoM simulations," *Journal of Automation, Mobile Robotics and Intelligent Systems*, vol. 10, pp. 3–8, 06 2016.

[11] SIMPLIS Technologies Inc., "Magnetics Design Module (MDM)," https://simplis.com/products/mdm, 2022.